INTERNATIONAL JOURNAL FOR NUMERICAL AND ANALYTICAL METHODS IN GEOMECHANICS, VOL. 22, 245–261 (1998)

A CONTINUUM MODEL OF LAYERED ROCK MASSES WITH NON-ASSOCIATIVE JOINT PLASTICITY

D.P. ADHIKARY* AND A .V. DYSKIN

Department of Civil Engineering, The University of Western Australia, Nedlands 6907, Australia

SUMMARY

Layered rock masses can be modelled either as standard, orthotropic continua if the layer bending can be neglected or as Cosserat continua if the influence of layer bending is essential. This paper presents a finite element smeared joint model based on the Cosserat theory. The layers are assumed to be elastic with equal thickness and equal mechanical properties. All the cosserat parameters are expressed through the elastic properties of layers, layer thickness and joint stiffness. Plastic-slip as well as tensile-opening of layer interface (joint) are accounted for in a manner similar to the conventional non-associative plasticity theory.

As an application, the behaviour of an excavation in a layered rock mass is examined. The displacement and stress fields given by smeared joint models based on the Cosserat continuum and the conventional anisotropic continuum approaches are compared with those obtained from the discrete joint model. The conventional anisotropic continuum model is found to break-down completely when the effective shear modulus in the direction parallel to layering is low in comparison to the shear modulus of the intact layer, whereas the Cosserat model is found to be capable of accurately reproducing complex load–deflection patterns irrespective of the differences in shear moduli. © 1998 John Wiley & Sons, Ltd.

Int. J. Numer. Anal. Meth. Geomech., Vol. 22, 245–261 (1998)

Key words: Cosserat continuum model; equivalent continuum medium; layered rock mass; finite element method; non-associative plasticity

1. INTRODUCTION

Rock mass in nature is generally traversed by multiple planes of weakness which separate it into blocks or layers. Such planes of weakness can be attributed to the geological depositional and rock forming processes. In many cases, rock masses are found to be intercepted by only one set of planes of weakness (e.g. joints and bedding planes) giving rise to stratification in the rock mass. The spacing of the planes of weakness (which hereafter will be denoted as joints) in a rock mass varies from a few centimetres to a few meters. Occurrence of such a stratified rock mass for a mineral deposit is not uncommon in mining applications. The main characteristics of these stratifications are their persistence and planar geometry.

Stratification in a rock mass results in highly anisotropic strength and deformation characteristics. This makes it necessary to include effects of joints into the mathematical formulations

*Correspondence to D. P. Adhikary, Geomechanics Group, Department of Civil Engineering, The University of Western Australia, Nedlands 6907, Australia

CCC 0363–9061/98/040245–17$17.50

Received 3 December 1996
Revised 11 July 1997

describing the load–deflection behaviour. When the number of joints within the problem domain is not large they can be considered individually in engineering analysis. This gives rise to discrete modelling where the intact layers and the joints are modelled explicitly by defining each layer and each joint individually. Calculations are performed either by introducing special joint elements into finite element models (e.g. References 1 and 2), or inter-layer boundaries into boundary element and distinct element models (e.g. References 3 and 4).

The joint element considered in Reference 1 has zero thickness and differs significantly from solid elements in their formulation. The thin layer element considered in Reference 2 is basically a solid element with its properties assigned in such a way that it closely simulates the behaviour of a joint. Recently, Desai and Ma[5] introduced a so-called Disturbed State Concept (DSC) in modelling of joint and interface behaviour. This approach includes provision for non-associative characteristics and anisotropy for joints.

On the other hand, in many cases, closely spaced joints occur in large numbers, which make the discrete modelling of such a rock mass almost an impossible task to perform. The only feasible way to incorporate the influence of such a system of joints in analysis is to formulate an equivalent continuum with appropriately modified properties accounting for the presence of joints.

This can be achieved as long as consistency and statistical homogeneity in joint properties and spacing can be established. Such a model remains valid when the joint spacing is much smaller than the characteristic length of the external stress variations and provides a large-scale (average) description of the material response to loading. The equivalent continuum implicitly incorporates within itself all the salient features of the material micro-structure without a need for their discrete description. This approach is often known as smeared (implicit) joint model in a sense that the joints are considered to be virtually smeared across the mass, i.e. the effects of the joints are implicit in the choice of stress–strain model adopted for the equivalent continuum. A distinctive advantage of the smeared joint model is that the problem region now can be discretized with a coarser mesh (i.e. subdivided into fewer finite elements) than in the discrete models where the size of the finite elements cannot exceed the layer thickness. Thus, in smeared models, the size of the finite elements is solely dictated by computational needs rather than by the layer thickness.

A layered material can be represented by a smeared joint model based on the conventional anisotropy theory[6–9] provided that no relative displacement takes place on joints. However, in the case, when the joint shear stiffness, in comparison to the shear stiffness of the intact layers, is either initially very low or becomes lower during loading, the models based on conventional anisotropy theory must be viewed with some caution. Depending upon geometry of the problem, the reduction in joint shear stiffness may induce sliding along the joints, thus causing layers to bend. Consider, for example, the case of a slope constructed in a layered rock mass (Figure 1(a)). In this case, the bending of the layered medium will create bending moments in addition to the conventional stresses.

The bending will introduce non-uniform stresses in the layers (Figure 1(b)). Since the stresses are averaged over the volume elements in the process of continuum formulation, the stress non-uniformity will vanish. However, the bending moments associated with the stress non-uniformity will remain coherent within a volume element and will not vanish upon averaging. Thus, in such cases, incorporation of moment stresses in a model becomes a must. Since the bending stiffness of the intact layers is neglected in conventional theories and moreover the bending induced stress non-uniformity vanishes upon averaging, such theories will lack

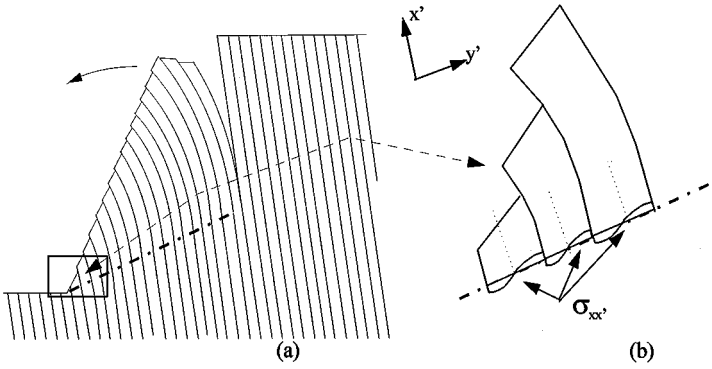

Figure 1. A schematic of bending induced stress non-uniformity in a layered rock mass: (a) a cartoon diagram of flexural toppling of a layered (foliated) rock slope; and (b) a diagram showing bending induced tensile and compressive stresses in rock layers

in their capabilities to accurately model the behaviour of layered materials with bending stiffness.

In a layered material with bending stiffness, relative joint displacement results in asymmetric macroscopic shear stresses which are physically equilibrated by bending moments. Hence, in describing the behaviour of a layered material with bending stiffness, it is necessary to incorporate an extra equilibrium equation balancing the differences in the shear stresses by bending moment in addition to the conventional force equilibrium equations. In such conditions, bending moments and associated rotations become additional independent variables and the models based on micro-polar theories, which include rotation and moment stresses as independent variables in their formulations, become more applicable. Cosserat brothers[10] presented such a theory of asymmetrical elasticity in 1909.

The Cosserat theory of elasticity incorporates a local rotation of material points in addition to the translation assumed in the classical elasticity, and couple (moment) stresses (moments per unit area) in addition to the classical force stresses (forces per unit area). The idea of couple stresses can be traced back to Voigt[11]. A substantial development in the Cosserat theory has taken place after 1958.[12–16] Mühlhaus and co-workers[17–19] (and see also the references cited there) have extensively developed the Cosserat theory in relation to layered material.

In References 19 and 20, a Cosserat model was formulated for the case of elastic joints. A Cosserat model with elastoplastic joints was formulated in Reference 21, where the Cosserat shear moduli were adjusted incrementally as soon as the joint yield criterion was attained. However, in that formulation, the effect of joint dilation was ignored. In the present study, the effect of joint dilation is taken into account by formulating equivalent Cosserat elastoplastic stiffness matrix in a manner similar to conventional non-associative elastoplasticity theory (see also Reference 22).

Desai[23] has introduced a new model based on the disturbed state concept (DSC) which allows for relative translation and rotation between the material clusters. Recently, Desai *et al.*[24] have shown that the model based on DSC approach remains mesh independent and can be used to model size effects and non-local effects. However, no direct comparison with the DSC-based model is made in this study.

2. COSSERAT THEORY

2.1. Cosserat deformation measures

This study is based on the following assumptions: (a) the intact layers are perfectly elastic, homogeneous and isotropic; (b) the joints are planar and the mechanical properties of each discrete joint are equal; (c) the layer thickness (joint spacing) is constant and much smaller than the characteristic length of the external stress variations; (d) the deformation and the curvature measures are infinitesimal; (e) the plane strain conditions can be assumed; and (f) the behaviour is time-independent.

Let us assume that the deformation quantities are infinitesimal and assign a local rigid cross to every material point (x, z) of the body in a Cartesian co-ordinate system (X, Z). In the process of deformation, the material points (rigid crosses) are rotated by an angle Ω_y about the y-axis in addition to the conventional displacement vector $\mathbf{u}(u, w)$. The rotation Ω_y is considered to be independent of $\mathbf{u}$ and differs from the classical rigid-body rotation ω_y, where

$$\omega_y = 1/2(\partial w/\partial x - \partial u/\partial z) \tag{1}$$

The classical theory yields the following strain tensor:

$$\varepsilon_{ij} = 1/2(\partial u_i/\partial x_j + \partial u_j/\partial x_i) \tag{2}$$

where, $i, j = 1, 2$, $x_1 = x$, $x_2 = z$, $\varepsilon_{11} = \varepsilon_{xx}$, $\varepsilon_{22} = \varepsilon_{zz}$ and so on.

In addition to the classical strain tensor ε_{ij}, there is an additional deformation quantity,

$$\Omega_y^{\mathrm{rel}} = \omega_y - \Omega_y \tag{3}$$

which represents the relative rotation between the material element and the associated rigid co-ordinate cross (in 2D case, there is only one component of rotation). In this case, the deformation tensor can be expressed by the distortion vectors,

$$\gamma_{xx} = \partial u/\partial x, \qquad \gamma_{zx} = \partial u/\partial z + \Omega_y \tag{4}$$

$$\gamma_{zz} = \partial w/\partial z, \qquad \gamma_{xz} = \partial w/\partial x - \Omega_y \tag{5}$$

and by the vector representing the measure of relative rotation between the neighbouring rigid crosses,

$$\kappa_x = \partial \Omega_y/\partial x, \qquad \kappa_z = \partial \Omega_y/\partial z \tag{6}$$

The conventional strain tensor can be expressed as the symmetrical part of the distortion tensor,

$$\varepsilon_{ij} = 1/2(\gamma_{ij} + \gamma_{ij}) \tag{7}$$

where $i, j = x, z$ and the relative rotation is

$$\Omega_y^{\mathrm{rel}} = 1/2(\gamma_{xz} - \gamma_{zx}) \tag{8}$$

2.2. The equilibrium equations

In the Cosserat theory, the couple (moment) stresses are incorporated additionally to characterise the internal stress state of the medium. Figure 2 presents a diagram showing stresses and volume forces acting on an infinitesimal element of the Cosserat continuum.

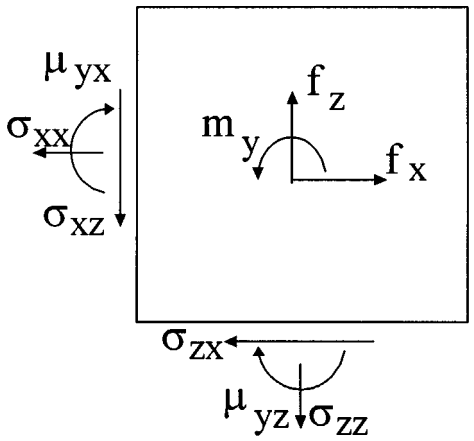

Figure 2. Stresses, volume forces and moments acting on a Cosserat element

The force-equilibrium equations remain the same as in the classical theory, i.e.,

$$\frac{\partial \sigma_{xx}}{\partial x} + \frac{\partial \sigma_{zx}}{\partial z} + f_x = 0 \tag{9}$$

$$\frac{\partial \sigma_{xz}}{\partial x} + \frac{\partial \sigma_{zz}}{\partial z} + f_z = 0 \tag{10}$$

while the introduction of moment stresses leads to the following moment equilibrium equation:

$$\frac{\partial \mu_{yx}}{\partial x} + \frac{\partial \mu_{yz}}{\partial z} + \sigma_{xz} - \sigma_{zx} + m = 0 \tag{11}$$

Here, μ_{yx} and μ_{yz} are the couple stresses and f_x, f_z and m are the body forces and the internal body moment. It is seen now that the ordinary stress tensor is no longer symmetric. However, if the moments are neglected, equation (11) yields $\sigma_{zx} = \sigma_{xz}$ and the situation reduces to the conventional theory.

2.3. Constitutive relationships for layered rock masses

In the expression of elastic energy, the four non-symmetric stress components σ_{xx}, σ_{zz}, σ_{zx}, σ_{xz} are conjugate to the four non-symmetric deformation components γ_{xx}, γ_{zz}, γ_{zx}, γ_{xz} and the moment stress μ_{yx} is conjugate to κ_x (here, $\mu_{yz} = 0$ as the layers are considered uniform in the direction of layering[19]). The relationship for the normal stress terms remains essentially the same as in the case of a conventional elastic medium, but the shear stress–strain relationship will be different. In addition, a relationship between the moment stress and the Cosserat rotation also exists. In order to account for the non-elastic cases, an incremental form of the constitutive relationships can be conveniently expressed through pseudo-vectors using the matrix notations as follows:

$$\dot{\boldsymbol{\sigma}} = [D_e]\dot{\mathbf{e}}_e \tag{12}$$

where

$$\boldsymbol{\sigma} = \{\sigma_{xx}, \sigma_{zz}, \sigma_{zx}, \sigma_{xz}, \mu_{yx}, \mu_{yz}\} \tag{13}$$

$$\mathbf{e} = \{\gamma_{xx}, \gamma_{zz}, \gamma_{zx}, \gamma_{xz}, \kappa_x, \kappa_z\} \tag{14}$$

The vector **e** will be further called the deformation vector and the dot over the field stands for the time differentiation and

$$D_e = \begin{bmatrix} A_{11} & A_{12} & 0 & 0 & 0 & 0 \\ & A_{22} & 0 & 0 & 0 & 0 \\ & & G_{11} & G_{12} & 0 & 0 \\ & & & G_{22} & 0 & 0 \\ & \text{symm} & & & B_1 & 0 \\ & & & & & 0 \end{bmatrix} \tag{15}^{\dagger}$$

where A_{11}, A_{12} and A_{22} are the conventional anisotropic elastic moduli and G_{11}, G_{12}, G_{22} and B_1 are the new Cosserat moduli. For a layered material, the constants A_{11}, A_{12} and A_{22} can be expressed as[22]

$$A_{11} = \frac{E}{1 - v^2 - \dfrac{v^2(1+v)^2}{1 - v^2 + E/bk_n}} \tag{16}$$

$$A_{12} = \frac{v/(1-v)}{\dfrac{1 - v - 2v^2}{E(1-v)} + \dfrac{1}{bk_n}} \tag{17}$$

$$A_{22} = \frac{1}{\dfrac{1 - v - 2v^2}{E(1-v)} + \dfrac{1}{bk_n}} \tag{18}$$

where E is the Young's modulus of layers, v is the Poison's ratio, k_n is the joint normal stiffness and b is the layer thickness (i.e. joint spacing).

In the case when the joints are modelled by very thin elastic inserts between the layers, the additional Cosserat constants can easily be expressed through the joint shear stiffness k_s, intact layer shear stiffness and G, and the flexural rigidity of the layers D_f.[19,20]

$$\frac{1}{G_{11}} = \frac{1}{G} + \frac{1}{bk_s} \tag{19}$$

$$G_{11} = G_{12} = G_{21} \tag{20}$$

$$G_{22} = G_{11} + G \tag{21}$$

and

$$B_1 = \frac{D_f}{b}\left(\frac{G - G_{11}}{G + G_{11}}\right) \tag{22}$$

†Note: Though the determinant of the stiffness matrix D_e (equation (15)) equals to zero, the material stiffness matrix (equation (30)) remains a non-singular matrix with a definitive determinant. The material stiffness matrix becomes singular only when the layers have a zero shear stiffness.

where

$$G = \frac{E}{2(1+\nu)} \tag{23}$$

and

$$D_{\mathrm{f}} = \frac{Eb^3}{12(1-\nu^2)} \tag{24}$$

Thus, for the layered rock masses, all the Cosserat parameters are expressed in terms of the elastic properties of layers, layer thickness and the joint shear and normal stiffnesses.

In the case when joint slip occurs, the situation becomes more complicated as a transition of elastic–plastic type will take place. In this study a very simple case of joint behaviour is considered. The joints are assumed to be rigid before sliding such that when sliding does not occur the joints do not influence the deformation and the material simply reduces to the conventional elastic, isotropic medium. When sliding over the joints occurs, the corresponding part of the material falls into the Cosserat state which is the case of a zero joint stiffness. This behaviour is of an ideal-plastic type with the only difference that the joint slip does not necessarily go indefinitely as for example in the case of conventional smeared (implicit) joint models. In this case, the sliding can be restrained by the bending rigidity. Thus, the Cosserat model has a potential for addressing situations where the conventional smeared joint approach may completely break down.

As in conventional elastoplasticity, the vector of deformation rate will be decomposed into an elastic $\dot{\mathbf{e}}_{\mathrm{e}}$ and a plastic part $\dot{\mathbf{e}}_{\mathrm{p}}$:

$$\dot{\mathbf{e}} = \dot{\mathbf{e}}_{\mathrm{e}} + \dot{\mathbf{e}}_{\mathrm{p}} \tag{25}$$

Equations (12) and (25) yield

$$\dot{\boldsymbol{\sigma}} = [D_{\mathrm{e}}](\dot{\mathbf{e}} - \dot{\mathbf{e}}_{\mathrm{p}}) \tag{23}$$

The conditions of the transition between the classical elastic and the Cosserat states will be formulated depending upon whether the joint yield limit is mobilised in tension or shear. Here, compression is assumed to be positive and the joints are assumed to possess zero tensile strength, hence tensile stresses in the directions normal to joints are not allowed. The tensile yielding is defined by the associative flow rule, where the joint yield criterion f_{t} and plastic potential function g_{t} can be expressed as

$$f_{\mathrm{t}} = \sigma_{zz} \geqslant 0 \quad \text{and} \quad g_{\mathrm{t}} = \sigma_{zz} \geqslant 0 \tag{27}$$

The shear yield function for the joints is defined by a non-associative flow rule, where the interface yield criterion f_{s} and plastic potential function g_{s} are expressed as

$$f_{\mathrm{s}} = |\sigma_{zx}| - (c_j + \sigma_{zz}\tan\varphi_j) \leqslant 0 \quad g_{\mathrm{s}} = |\sigma_{zx}| - \sigma_{zz}\tan\psi_j + \mathrm{const} \leqslant 0 \tag{28}$$

Here, c_j is the joint cohesion, ϕ_j is the joint friction angle and ψ_j is the joint dilation angle. In a manner similar to the conventional plasticity theory the rate of plastic deformation is assumed to be equal to

$$\dot{\mathbf{e}}_{\mathrm{p}} = \dot{\lambda}\frac{\partial g}{\partial \dot{\boldsymbol{\sigma}}} \tag{29}$$

where $\dot{\lambda}$ is the so-called plastic multiplier. Then, as usual, the elasto–plastic stiffness matrix D_{ep} can be expressed in the form

$$D_{ep} = D_e - \alpha \frac{D_e \left\{\frac{\partial g}{\partial \dot{\boldsymbol{\sigma}}}\right\} \left\{\frac{\partial f}{\partial \dot{\boldsymbol{\sigma}}}\right\}^T D_e}{\left\{\frac{\partial g}{\partial \dot{\boldsymbol{\sigma}}}\right\}^T D_e \left\{\frac{\partial f}{\partial \dot{\boldsymbol{\sigma}}}\right\}} \tag{30}$$

such that

$$\dot{\boldsymbol{\sigma}} = [D_{ep}]\dot{\mathbf{e}} \tag{31}$$

Here α is defined as

$$\alpha = 1 \quad \text{if } f_s = 0 \quad \text{and} \quad \dot{\lambda} > 0, \qquad 0 \text{ if } f_s < 0 \quad \text{and/or} \quad \dot{\lambda} \leqslant 0 \tag{32}$$

3. FINITE ELEMENT FORMULATION

From the principle of virtual work, it follows that[19]

$$\int_B (\sigma_{ij}\delta\varepsilon_{ij} + \mu_{yi}\delta\kappa_i)\mathrm{d}V = \int_{\partial_1 B} t_i \delta u_i \,\mathrm{d}A + \int_{\partial_2 B} m\delta\Omega_y \,\mathrm{d}A \tag{33}$$

where $\sigma_{ij}n_j = t_i \quad \text{on } \partial_1 B, \qquad m_i n_i = m \quad \text{on } \partial_2 B, \quad i, j = (x, z)$ (34)

From equations (13), (14) and (33), the principle of virtual work can be expressed as

$$\int_B \boldsymbol{\sigma}^T \delta\mathbf{e}\,\mathrm{d}V = \int_{\partial_T B} \mathbf{r}^T \delta\mathbf{U}\,\mathrm{d}A \tag{35}$$

where

$$\mathbf{r} = [t_x, t_z, m] \tag{36}$$

$$\mathbf{U} = [u, w, \Omega_y] \tag{37}$$

The incremental form of equation (35) for solving non-linear problems can be written as

$$\sigma_{t+\Delta t} = \Delta\sigma + \sigma_t \tag{38}$$

and

$$\Delta\sigma = D_{ep}\Delta e \tag{39}$$

The distribution of displacements and rotations within the domain B_e of a finite element can be expressed as

$$U = \phi_N U_N, \quad \delta U = \phi_N \delta U_N, \qquad N = 1, 2, \ldots, N^e \tag{40}$$

where ϕ_N are the shape functions, N is the node number and N^e is total number of nodal points in each element which in this study equals to 8 as each finite element is represented by a 8-noded isoparametric quadrilateral.

Although, for the conventional continuum model with only two translational degrees of freedom, a 2×2 integration rule would provide a convergent solution when special measures are taken to suppress the zero energy modes resulting from reduced 2×2 quadrature, this is not true

for the Cosserat medium which possesses an additional (rotational) degree of freedom. Consequently, the numerical spatial integration has been conducted with a 3×3 quadrature. Since the same order of derivatives of translational displacements and the rotations is involved in the governing equations, the same shape functions (a complete quadratic polynomial plus the monomial terms x^2y and xy^2) are used for the interpolation of the displacements and rotations. Another option would be to interpolate the rotations with a linear polynomial only, however that option has not been studied here.

The deformation vector $\mathbf{e}$ can be computed as:

$$\mathbf{e} = B_N U_N \tag{41}$$

where B_n is the following strain–displacement matrix:

$$[B_n] = \begin{bmatrix} \phi_{N,x} & 0 & 0 \\ 0 & \phi_{N,z} & 0 \\ \phi_{N,z} & 0 & \phi_N \\ 0 & \phi_{N,x} & -\phi_N \\ 0 & 0 & \phi_{N,x} \\ 0 & 0 & \phi_{N,z} \end{bmatrix} \tag{42}$$

From equations (35), (39) and (41) we obtain

$$(\delta U_N)^{\mathrm{T}} K^{NM} \Delta U_M = (\delta U_N)^{\mathrm{T}} (F_N^{\mathrm{ext}} - F_N^{\mathrm{int}}) \tag{43}$$

where

$$K^{NM} = \int_{B^e} (B_N)^{\mathrm{T}} D_{\mathrm{ep}} B_M \, \mathrm{d}V \tag{44}$$

is the tangent stiffness matrix,

$$F_N^{\mathrm{ext}} = \int_{\partial_1 B^e} t\phi_N \, \mathrm{d}A \quad \text{or} \quad \int_{\partial_2 B^e} m\phi_N \, \mathrm{d}A \tag{45}$$

is the generalized external load vector, and

$$F_N^{\mathrm{int}} = \int_{B^e} (B^N)^{\mathrm{T}} \sigma_t \, \mathrm{d}V \tag{46}$$

is the generalized initial force vector.

4. EXAMPLE PROBLEMS

The application of the Cosserat continuum model to the problem of flexural toppling failures of foliated rock slopes has been considered by Adhikary *et al.*[21] This study will consider some numerical examples specifically aimed at verifying the capability of this model to predict the load–deformation response of excavations in a layered rock mass. To conduct numerical calculations, the Cosserat model has been incorporated into the finite element code AFENA.[25] The example problems are analysed using the Cosserat FE code, FE code based on conventional

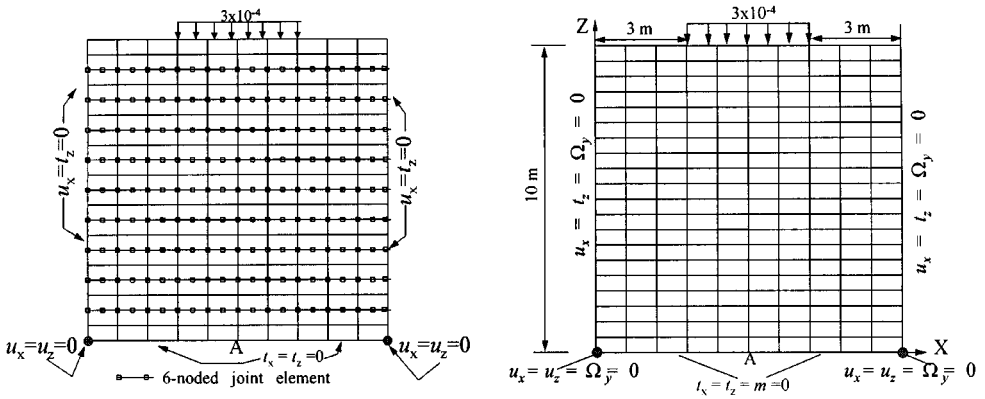

Figure 3. Finite element mesh and boundary conditions in Example 1

anisotropy theory and discrete joint FE code where each joint is modelled explicitly. Here, the discrete joint FE calculations are used as bench-marks for the verification of the Cosserat FE calculations. In the examples considered, the problem region consisted of ten 1 m-thick horizontal rock layers with Poisson's ratio of 0·2. For the sake of simplicity, the stress and the stiffness parameters of the rock has been normalized against the Youngs modulus, E, of rock layers. Thus, the computed results corresponds to the Youngs modulus of 1.

Example 1. This example is designed to show, firstly, the importance of layer bending stiffness and, secondly, to verify the capability of the Cosserat model and the model based on conventional anisotropy theory (implicit joint model) to accurately predict the load deflection behaviour of the layered rock mass. Here, the joints are assumed to be elastic and joint normal stiffness k_n/E is assumed to be $10^8\ \mathrm{m}^{-1}$. Several calculations are conducted for the case of different joint shear stiffness varying from very high value of $k_s/E = 10^8\ \mathrm{m}^{-1}$ to as low as $k_s/E = 10^{-1}\ \mathrm{m}^{-1}$.

The model geometry, finite element mesh and the boundary conditions used in this example are shown in Figure 3. Instead of a uniformly distributed stress field, this configuration is chosen to quantify the prediction capability of smeared joint models even under non-uniformly distributed external stresses. Since substantial layer bending is expected in the examples to follow, each of the problem domain is divided into 200 8-noded isoparametric elements. This element has 24 degrees of freedom because each of 8 nodes has three degrees of freedom: two translations and one rotation.

In discrete modelling, each layer is discretised into 20 8-noded isoparametric quadrilateral, each joint (inter-layer interface) is discretised into 10 6-noded joint elements and numerical spatial integration is conducted with a 2×2 quadrature. The load P/E of 3×10^{-4} is applied in one increment.

Figure 4 shows comparisons of the displacements of the point A (marked in Figure 3) as obtained from the three models for the linear elastic case as a function of the effective shear modulus G_{11}. It is seen that the Cosserat model accurately predicts the load deflection behaviour irrespective of the joint shear stiffness values (which determines the effective shear modulus), whereas the anisotropic model deviates substantially from the true behaviour, as soon as the

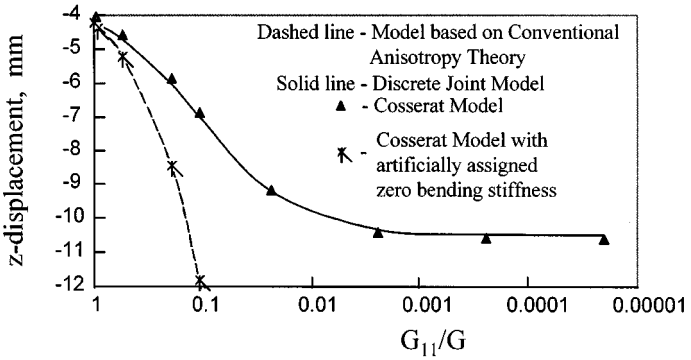

Figure 4. Comparison of vertical displacement of location A (Figure 3) obtained from different models in Example 1

effective shear modulus in the direction of layering becomes less than the intact rock shear modulus. This is not surprising as the layers in the anisotropic model possess no bending stiffness; correspondingly the model over-predicts the layer deflection.

A set of separate calculations are conducted using the Cosserat model where the intact rock layers are artificially assigned with zero bending stiffness. As can be seen from Figure 4, the Cosserat calculations in this case coincides with the conventional anisotropic model calculations. Thus, it is obvious that the conventional anisotropic model can be used only in the cases when the layer bending stiffness can be neglected.

Example 2. This example is designed to verify the capability of the Cosserat model to represent the true behaviour of layered rock masses where joints undergo elasto-plastic deformation. For this reason, a sequential excavation in a layered rock mass is considered. Three joint friction angles are adopted, i.e. $\varphi_j = 0^\circ$, 10° and 30°. Dilation angle of 20° is used in the case of joint friction angle of 30° and for all other friction angles it is assumed to be zero. In all calculations, both k_n/E and k_s/E are initially assumed to be 10^8 m^{-1}. A uniformly distributed load (3×10^{-4}) is applied on a span equivalent to four-layer thickness.

The discrete joint and the Cosserat finite element meshes and the boundary conditions used in each example are shown in Figure 5. Since substantial layer bending is expected in the examples to follow, each of the smeared joint problem domains is divided into 200 8-noded isoparametric elements. In discrete modelling, each layer is discretized into 20 8-noded isoparametric quadrilaterals, each joint (inter-layer interface) is discretized into 10 6-noded joint element. Numerical spatial integration is conducted in the same way as mentioned above. Once the load of 3×10^{-4} is applied, a rectangular hole is excavated in the centre of the problem domain in stages numbered 2–9 in Figure 6.

Figures 7–9 show the cumulative displacements of the floor of the excavation, the roof of the excavation and the centre of the loaded area as marked in Figure 6 by *A*, *B*, *C* respectively. It can be seen that the displacement patterns obtained from the Cosserat and the discrete joint models are very similar irrespective of the joint friction angles, whereas the displacement patterns obtained from the conventional anisotropic model starts to deviate substantially as the joint friction angle is reduced.

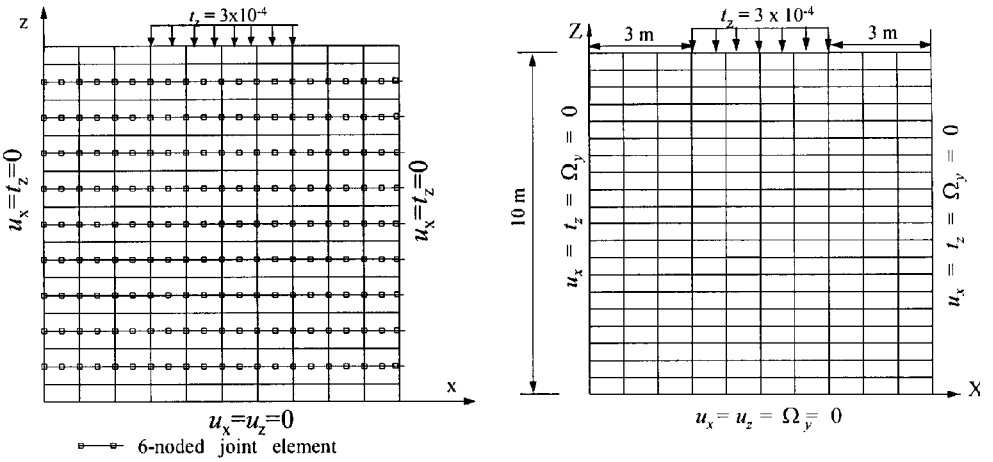

Figure 5. Cosserat FE mesh and boundary conditions in Example 2

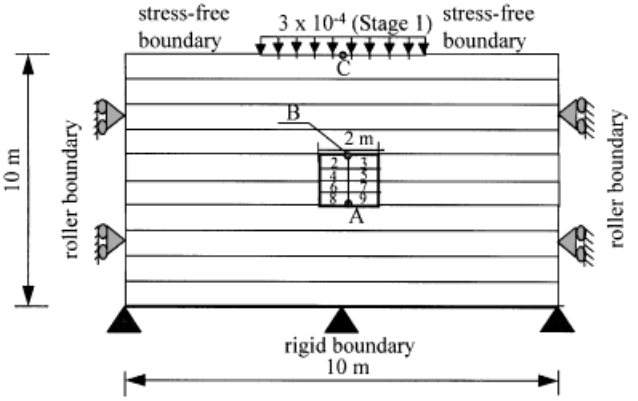

Figure 6. A schematic diagram of the problem (Example 2)

In the case of joint friction angle of 0°, the Cosserat model and the discrete joint model results are remarkably similar with a maximum difference of 2·5 percent. On the other hand, the anisotropic model became numerically unstable so no solution can be obtained. This is due to the fact that unrestrained sliding may occur in the anisotropic model with a zero effective shear modulus, whereas, in the Cosserat case, it is restrained by the bending rigidity. Thus, the Cosserat model has the potential of addressing the situations where the conventional anisotropic joint approach may break down completely.

In the case of the joint friction angle of 10°, a maximum difference of 5·9 percent at location *B* is observed between the results of the Cosserat and the discrete joint models. The displacements obtained from the anisotropic model still differ substantially from those of the discrete model (Figure 8(b)).

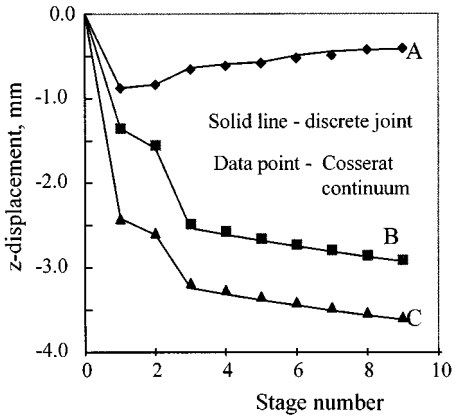

Figure 7. Comparison of vertical displacements in Example 2 ($\varphi_j = 0°, \psi_j = 0°$). (Note: the anisotropic model is unstable in this case)

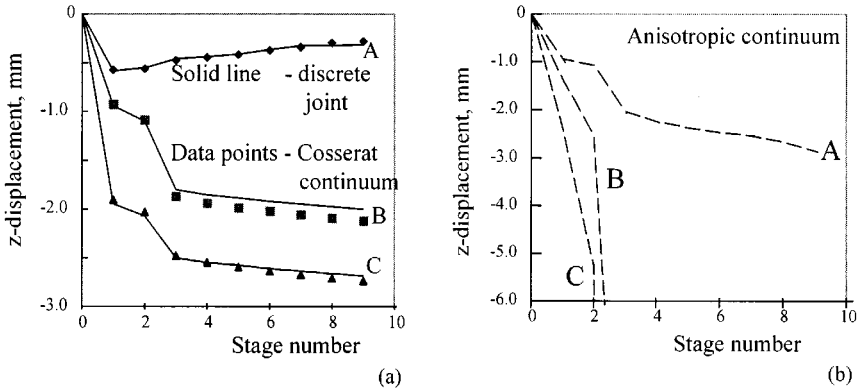

Figure 8. Comparison of vertical displacements in Example 2 ($\varphi_j = 10°, \psi_j = 0°$). (Note: the results of the anisotropic model are separately shown)

In the case of joint friction angle of 30°, the predictions of all the three models are remarkably similar except for the location *B* where a maximum difference in vertical displacement of about 5·8 percent is observed between the Cosserat model and the discrete joint model results and a difference of about 24% is obtained in the case of anisotropic model. In this case, most of the layer interfaces (joints) remained rigid (i.e. no plastic slip took place) except at immediate vicinity of the roof of the excavation resulting in a minimal differences in shear moduli within a larger area of the problem region. This is evident from Figure 9 where the displacements obtained from an isotropic model are also plotted. The results of the isotropic model matches to those of the discrete model quite perfectly with minor differences in the roof region indicating the development of a plastic zone. This is why the conventional anisotropic model results in this case are fairly accurate everywhere except of the roof region, where it still shows considerably less accuracy than the Cosserat model.

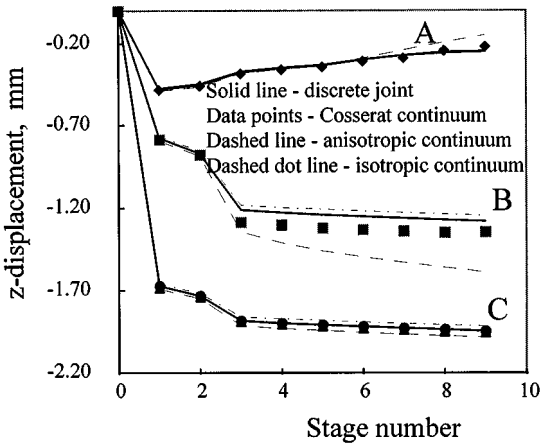

Figure 9. Comparison of vertical displacements in Example 2 ($\varphi_j = 30^\circ, \psi_j = 20^\circ$)

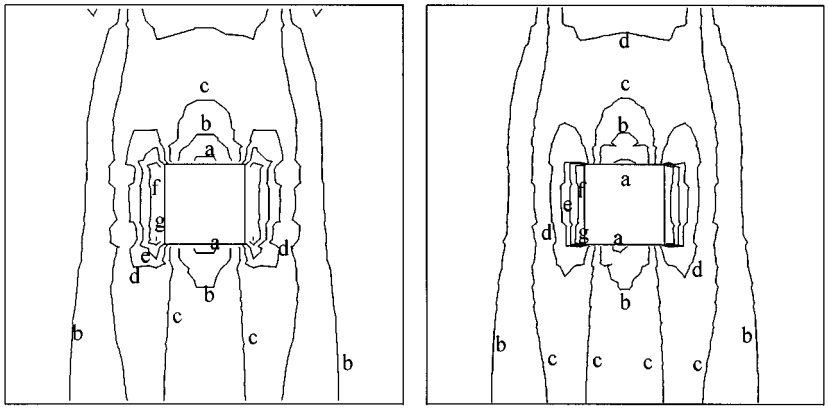

Figure 10. Comparison of vertical stress contours (σ_{zz}/E) at end of stage 9 in Example 2 ($\varphi_j = 0^\circ, \psi_j = 0^\circ$)

Figure 10 presents contours of the vertical stress component for the case of zero joint friction angle and zero dilation angle, which shows remarkable similarities between the Cosserat and the discrete joint models. Figures 11 and 12 present the vertical stress contours obtained from the three models for the case of the joint friction angle of 30° and the joint dilation angle of 20° at the end of stage 6 and stage 9, respectively. The stress contours are similar in all three models, except for the roof and floor regions where the layer bending plays a major role. Thus, in these regions, the anisotropic model results are slightly different from those of the other two models.

Figure 13 presents a typical moment stress plot obtained from the Cosserat model for the case of zero joint friction and dilation angles. As can be seen, the maximum bending moment is localised at the centre of the roof indicating the possible location of the layer fracture initiation.

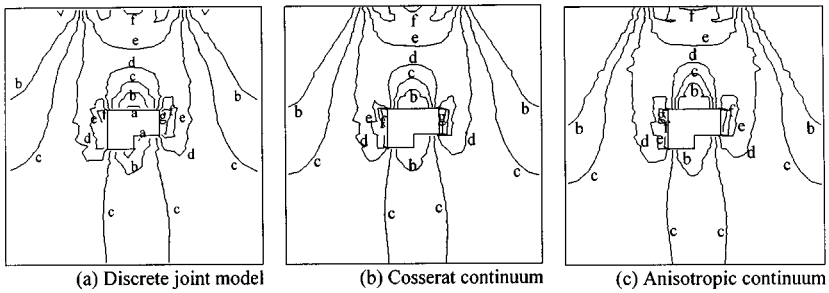

Figure 11. Comparison of vertical stress contours (σ_{zz}/E) at the end of stage 6 in Example 2 ($\varphi_j = 30^\circ, \psi_j = 20^\circ$)

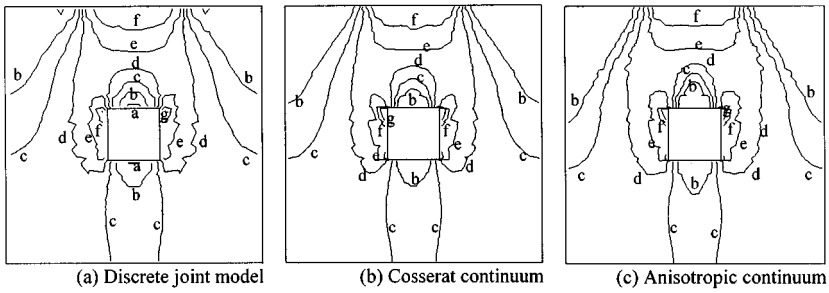

Figure 12. Comparison of vertical stress contours (σ_{zz}/E) at the end of stage 9 in Example 2 ($\varphi_j = 30^\circ, \psi_j = 20^\circ$)

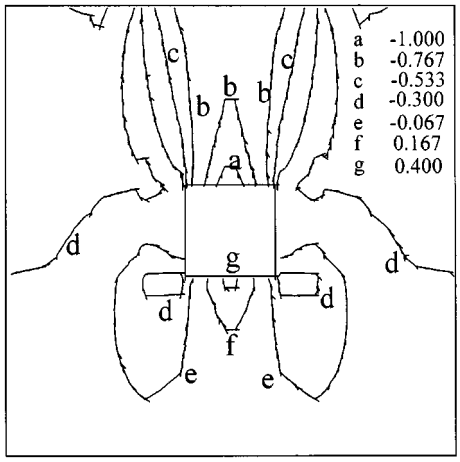

Figure 13. Normalised moment stress (μ_{yx}/Eb) plot in Example 2 ($\varphi_j = 0^\circ, \psi_j = 0^\circ$)

Knowing the moment stresses, the possibility of roof fracture can be easily estimated using the following expression.

$$\sigma_{\text{tensile}} = \frac{6\mu_{zx}(1-\nu^2)}{b} + \sigma^{\text{o}}_{xx} \tag{47}$$

where, σ_{tensile} is the microscopic tensile strength of the intact rock layer and σ^{o}_{xx} is the macroscopic stress component that can be obtained from the Cosserat model result.

5. CONCLUSIONS

In situations when the layer bending becomes important one needs to use the theories which include moment stresses in their formulations. Layered rock masses can be modelled as standard orthotropic continua only if the layer bending stiffness can be neglected.

In this study, the Cosserat model with non-associative joint plasticity has been implemented into a finite element code AFENA and the capability of such models to accurately predict the load–deformation behaviour of layered rock masses with bending stiffness is investigated. It is shown that the conventional anisotropic continuum model breaks down completely when the effective shear modulus becomes less than the intact rock layer shear modulus, whereas the Cosserat model accurately predicts the load–deflection behaviour irrespective of the differences in shear moduli.

Further to verify the capability of the Cosserat model to predict the load deflection behaviour of the layered rock mass with elastoplastic joints, an example of excavation in a layered rock mass is considered. The comparison with calculations conducted using the discrete joint model shows that the Cosserat model is capable of accurately reproducing complex load–deformation patterns. Maximum differences between the Cosserat and the discrete joint calculations are observed to be less than 6 percent which can be considered to be within the limit of numerical accuracy.

ACKNOWLEDGEMENTS

The authors are grateful to Prof. J. P. Carter of the University of Sydney for his permission to use the finite element program AFENA in this study, Dr. H.-B. Muhlhaus for discussion of the model, and Prof. M. F. Randolph for his support and encouragement. This work was supported by an Australian Research Council Full Grant (1996–1998).

REFERENCES

1. R. E. Goodman, R. L. Taylor and T. Brekke, 'A model for the mechanics of jointed rock', *J. Soil Mech. Found. Div., Proc. ASCE*, **94,** 637–659 (1968).
2. C. S. Desai, M. M. Zaman, J. G. Lightner and H. J. Siriwardane, 'Thin-layer element for interfaces and joints', *Int. J. Numer. Anal. Meth. Geomech.*, **8,** 19–43 (1984).
3. J. L. Meek and C. Dai, 'Development of the fundamental BEM solution for half space–near surface excavations', *Asia-Pacific Conf. on Comp. Mech.*, 1992.
4. P. A. Cundall and R. D. Hart, 'Numerical modelling of discontinua', *Engng. Comput.*, **9,** 101–113 (1992).
5. C. S. Desai and Y. Ma, 'Modelling of joints and interfaces using the disturbed state concept', *Int. J. Numer. Anal. Meth. Geomech.*, **8,** 19–43 (1984).
6. I. M. Lifstiz and L. N. Rosenzweig, 'On the theory of elastic properties of polycrystals', *JETP*, **16**(11) (1946), and Letter to the editor. On the theory of elastic properties of polycrystals, *JETP*, **21**(10) (1951).
7. M. D. G. Salamon, 'Elastic moduli of stratified rock mass', *Int. J. Rock Mech. Min. Sci. Geomech. Abstr.*, **5,** 519–527 (1968).

8. C. M. Gerrard, 'Elastic models of rock masses having one, two and three sets of joints', *Int. J. Rock Mech. Min. Sci. Geomech. Abstr.*, **19,** 15–23 (1982).
9. H. Alehossein and J. P. Carter, 'On the implicit and explicit inclusion of joints in the analysis of rock masses', in Rossmanith (ed.), *Mech. of Jointed and Faulted Rocks*, Balkema, Rotterdam, 1990, 487–494.
10. E. Cosserat and F. Cosserat, '*Theorie des corps deformables*', Hermann, Paris, 1909.
11. W. Voigt, 'Theoretische studien uber die elasticitatsverhaltnisse der krystalle', Abh. Ges. Wiss. Gottingen **34** (1887); Uber medien ohne innere Krafte and eine durch sie gelieferte mechanische Deutung der Maxwell-Hertzschen Gleichungen. *Gott. Abh.* (1894) 72–79.
12. G. Grioli, 'Elasticita Asimetrica' *Ann. di Mat. Pura ed. Appl.*, Ser. IV, **50,** 389–417 (1960).
13. C. Truesdell and R. A. Toupin, 'The classical field theories', *Encl. of Physics*, Vol. III (1), Secs. 200, 203, 205, Berlin-Gottingen-Heidelberg, 1960.
14. R. D. Mindlin, and H. F. Tiersten, 'Effects of couple stresses in linear elasticity', *Arch. Rational Mech. Anal.*, **11,** 415–448 (1962).
15. E. L. Aero and R. V. Kuvshinskii, 'Continuum theory of asymmetric elasticity—the problem of internal rotation', *Soviet Physics—Solid State*, **5**(9), 1892–1897 (1964).
16. C.-T. Sun, J. D. Achenbanch and G. Herrmann, 'Continuum theory for a laminated medium', *Trans. ASME*, Ser. E., *J. Appl. Mech.*, **35**(3), 467–475 (1968).
17. H.-B. Mühlhaus, 'Surface instability of a half plane with bending stiffness' (In German), *Ing. -Arch.*, **55,** 388–400 (1985).
18. H.-B. Mühlhaus, 'Stress and couple stress in a layered half plane with bending stiffness', *Int. J. Numer. Anal. Methods Geomech.*, **14,** 545–563 (1990).
19. H.-B. Muhlhaus, 'Continuum models for layered and blocky rock', *Comprehensive Rock Eng.*, Invited Chapter for Vol. II: Analysis and Design Methods, Pergamon Press, 209–230 (1993).
20. N. V. Zvolinskii and K. N. Shkhinek, 'Continual model of laminar elastic medium', *Mech. Solids*, **19**(1), 1–9 (1984).
21. D. P. Adhikary, A. V. Dyskin and R. J. Jewell, 'Numerical modelling of the flexural deformation of foliated rock slopes', *Int. J. Rock Mech. Min. Sci Geomech. Abstr.*, **33**(6), 611–616 (1996).
22. H.-B. Mühlhaus, 'A relative gradient model for laminated materials', in H.-B. Mühlhaus (ed.), *Continuum Models for Materials with Micro-Structure*, Chapter 13, 1995.
23. C. S. Desai, 'Constitutive modelling using the disturbed state concept', in H.-B. Mühlhaus (ed.), *Continuum Models for Materials with Micro-Structure*, Chapter 8, 1995.
24. C. S. Desai, C. Basaran and W. Zhang, 'Numerical algorithms and mesh dependence in the disturbed state concept', *Int. J. Numer. Meth. Engng.*, (1996), accepted.
25. J. P. Carter and N. G. Balaam, *AFENA Users' Manual*. Centre for Geotechnical Research, University of Sydney, Australia, 1995, Version 5.

